spectrum of the metal atom in a matrix,[11] there is a degree of uncertainty about their values in complexes. It would be helpful for photoelectron studies such as in ref 5b to focus on the energy range of the σ-framework electrons to look for this effect.

Our calculations place the metal CO π^* back-bonding levels about $^3/_4$ eV above the metal-ring π-bonding levels, an ordering in agreement with the Bursten-Fenske result[7c] and with the photoelectron analysis of Hall, Hillier, Connor, Guest, and Lloyd.[6b] The Bursten-Fenske separation is about twice ours and the two theoretical results bracket the experimental measurement. These results are in contradistinction to initial-state and final-state corrected Hartree-Fock results in ref 6b, and as discussed in that reference and in ref 7c, one must go beyond using a single determinant to produce the measured results with ab initio calculations.

Concluding Comments

We have found it possible to make a full determination of the structure of (cyclobutadiene)iron tricarbonyl using the ASED quantum-mechanical theory. We find, as did past workers using an orbital method and an assumed structure,[7c] that cyclobutadiene π e_g orbitals are stabilized by overlap with a metal d orbital of similar energy. Futher, we find that the *total* molecular orbital energy does not approximate accurately the energy surface for complexed cyclobutadiene, though it does for free cyclobutadiene. Thus the pairwise atom-atom repulsion component must be included in a full structure determination (in other theories this component corresponds approximately to the nuclear repulsion energy minus electron repulsion energies, which are counted twice). However, molecular orbital theory provides the general reasons for complex formation. We also find the cyclobutadiene 2s σ-framework a_1 orbital is stabilized in an interaction with an iron 4p orbital and that this contributes substantially to the energy. Experimental identification of this class of stabilization could be interesting.

Acknowledgment. We thank Standard Oil of Ohio (SOHIO) for supporting this work through a grant to the Case Western Reserve University Department of Chemistry. Professor W. von Philipsborn is thanked for arousing our curiosity about (cyclobutadiene)iron tricarbonyl.

Registry No. (Cyclobutadiene)iron tricarbonyl, 12078-17-0.

(11) Anderson, A. B. *J. Chem. Phys.* **1977**, *66*, 5108.

Contribution from the Department of Chemistry, University of Notre Dame, Notre Dame, Indiana 46556

Electronic Structure of Diiron Ferraboranes

E. L. ANDERSEN, R. L. DeKOCK,*[1] and T. P. FEHLNER*

Received November 3, 1980

The electronic structure of two metallaboranes containing the $Fe_2(CO)_6$ fragment, $Fe_2(CO)_6B_2H_6$ and 1,2-$[Fe(CO)_3]_2B_3H_7$, has been explored with the use of the experimental techniques of UV-photoelectron spectroscopy and UV-visible absorption spectroscopy. Quantum chemical calculations have been carried out on these molecules with use of the extended Hückel and Fenske-Hall methods. The assigned photoelectron spectra allow a comparison of the radical cation states for the series B_5H_9, 1-$Fe(CO)_3B_4H_8$, and 1,2-$[Fe(CO)_3]_2B_3H_7$, each molecule of which formally has 14 skeletal electrons. The experimental results demonstrate significantly different charges on the iron atoms in 1,2-$[Fe(CO)_3]_2B_3H_7$, and the calculations suggest that the charge difference is required by the cage geometry. That is, in close analogy with B_5H_9, it appears that the square-pyramidal cage geometry requires greater valence orbital participation in bonding for iron in an apical position vs. a basal position. Available evidence suggests the low-energy UV-visible absorption bands of diiron ferraboranes are associated with the $Fe_2(CO)_6$ fragment and that the lowest unfilled MO is Fe-Fe antibonding in nature.

Introduction

The primary measure of the nature of chemical bonding is molecular geometry. Hence, similar geometries imply related bonding. For this reason, the hypothesis, referred to as the "borane analogy",[2] that the cage structures of boranes should serve as models for some transition-metal clusters provides not only an appealing paradigm of pedagogical value but also a method of systematically exploring the electronic properties of transition metals in a cluster environment. In the molecular orbital (MO) approximation, an observed metal cluster-borane analogy implies qualitative similarities between the MO's associated with the cluster bonding. But it must be remembered that there will be many MO's in both borane and metal cluster, not primarily associated with cluster bonding, that are different. Thus, similar cluster geometries do not imply similar physical and chemical properties. Still the borane provides a useful base point against which the behavior of the metal systems can be contrasted.

In this vein we have set out to systematically explore the five-atom cluster system with 14 skeletal bonding electrons which, with iron as the transition metal, has the general molecular formula $[Fe(CO)_3]_xB_{5-x}H_{9-x}$. We have previously presented information on the electronic structure[3] and photochemistry[4] of 1-$Fe(CO)_3B_4H_8$[5] and on the geometrical structure of 1,2-$[Fe(CO)_3]_2B_3H_7$.[6] In the following, the electronic structure of 1,2-$[Fe(CO)_3]_2B_3H_7$ and the related compound $Fe_2(CO)_6B_2H_6$ is explored with use of UV-photoelectron (PE) spectroscopy to reveal the low-lying radical cation states and UV-visible spectroscopy to reveal the low-lying excited molecular states. With the aid of the extended Hückel[7] and Fenske-Hall[8] quantum chemical methods, the experimental information is discussed and used to construct a picture of the structure and bonding in these ferraboranes

(1) Department of Chemistry, Calvin College, Grand Rapids, MI 49506.
(2) Wade, K. *Adv. Inorg. Chem. Radiochem.* **1976**, *18*, 1. See also: Rudolph, R. W. *Acc. Chem. Res.* **1979**, *9*, 446. Grimes, R. N. *Ann. N.Y. Acad. Sci.* **1974**, *239*, 180.
(3) Ulman, J. A.; Andersen, E. L.; Fehlner, T. P. *J. Am. Chem. Soc.* **1978**, *100*, 456.
(4) Fehlner, T. P. *J. Am. Chem. Soc.* **1980**, *102*, 3424.
(5) Greenwood, N. N.; Savory, C. G.; Grimes, R. N.; Sneddon, L. G.; Davison, A.; Wreford, S. S. *J. Chem. Soc., Chem. Commun.* **1974**, 718.
(6) Andersen, E. L.; Haller, K. J.; Fehlner, T. P. *J. Am. Chem. Soc.* **1979**, *101*, 4390. Haller, K. J.; Andersen, E. L.; Fehlner, T. P. *Inorg. Chem.* **1981**, *20*, 309.
(7) Hoffmann, R. *J. Chem. Phys.* **1963**, *39*, 1397. Hoffmann, R.; Lipscomb, W. N. *Ibid.* **1962**, *36*, 2179, 3489; **1962**, *37*, 2872.
(8) Hall, M. B.; Fenske, R. F. *Inorg. Chem.* **1972**, *11*, 768. Hall, M. B. Thesis, University of Wisconsin, Madison, WI, 1971. Fenske, R. F. *Pure. Appl. Chem.* **1971**, *27*, 61.

0020-1669/81/1320-3291$01.25/0

Table I. Vertical Ionization Potentials, Relative Band Areas, Band Characters, and Eigenvalues[a] for $Fe_2(CO)_6B_2H_6$

band[b]	IP,[c] eV	A/E[d] (rel)	$A/E(736)/A/E(584)$[e]	IP's[f] per band	band[f] character	F-H[h] eigenvalues, eV	EHT[i] eigenvalues, eV
1	8.2 sh	0.3	0.8	7	Fe(3d), 7 B(2p), 1	$13b_2$, 3.60, LUMO	9.21
	8.8					$15a_1$, 8.44, HOMO (Fe-Fe)	10.29, B-B
	9.1					$14a_1$, 9.04, Fe(3d), B(2p)	11.13, Fe-Fe
2	10.1			1		$12b_2$, 10.65	11.86
						$8a_2$, 10.81	12.00
						$13a_1$, 11.34 Fe(3d)	12.10 Fe(3d)
						$9b_1$, 11.45	12.14
						$11b_2$, 11.47	12.20
						$12a_1$, 13.82, Fe(3d), B(2p)	12.55
3	11.9	0.4	[1.0]	4	B(2p) H(1s)	$10b_2$, 14.76	13.39
	12.8					$7a_2$, 15.64	13.81
						$11a_1$, 16.69 H_b-B-H_t	14.42 H_b-B-H_t
						$8b_1$, 16.74	14.50
4	14.3	1.0	0.6	18	CO(5σ, 1π)	18-22[g]	14-16 CO

[a] The signs of all eigenvalues have been changed from negative to positive for ease of comparison with IP's via Koopmans' theorem. [b] See Figure 3. [c] Vertical IP's; sh = shoulder. [d] HeI band area over mean electron energy. [e] [] defined as 1.0; 736 Å refers to Ne I and 584 Å to He I. [f] According to assignment described in text. [g] In the range 18-22 eV there are 20 eigenvalues; two of these have significant B-H character. [h] Fenske-Hall = F-H. [i] EHT = extended Hückel.

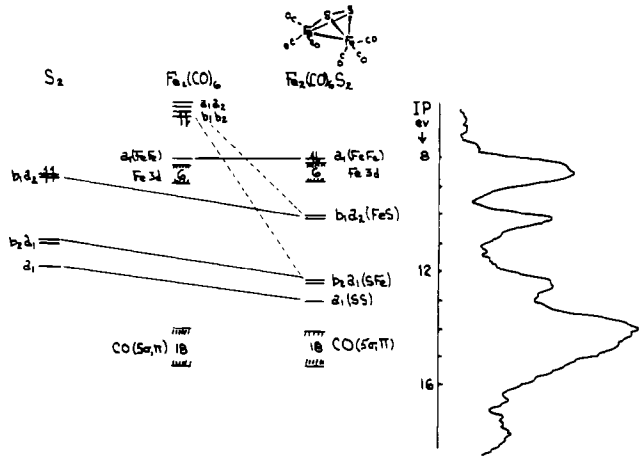

Figure 1. Correlation diagram to illustrate the formation of the occupied orbitals of $Fe_2(CO)_6S_2$ and the assignment of the corresponding radical cation states in the photoelectron spectrum.

within the confines of Koopmans' theorem.[9]

Results and Discussion

(I) Photoelectron Spectra. The two compounds discussed in this work contain the $Fe_2(CO)_6$ fragment with a bent-sawhorse-type structure. In order to characterize the behavior of this iron fragment in terms of its PE behavior, we have previously examined the spectrum of the $Fe_2(CO)_6S_2$ molecule.[10] Our knowledge of this molecule, summarized in Figure 1, is based both on a PE spectroscopic study as well as a quantum chemical analysis including the SCF-Xα-SW technique. The ionization potentials (IP's) associated with a given fragment can be divided into two types: those that transfer more or less unchanged from molecule to molecule containing the fragment and those that do not transfer unchanged. For $Fe_2(CO)_6$, the transferable IP's are the 6 Fe 3d IP's (essentially nonbonding) and the 18 CO ionizations (derived from the 5σ and 1π IP's of CO). There is one IP associated with the Fe–Fe bond that will be transferable if the corresponding orbital does not mix significantly with other orbitals of the molecule. In addition, four other valence IP's may have significant Fe 3d character, but in general these

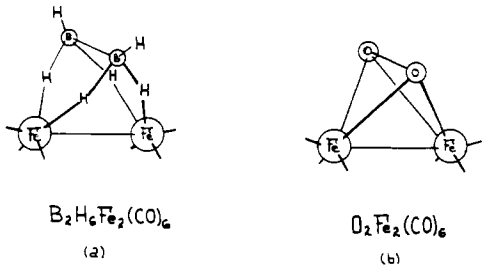

Figure 2. Proposed structure for $B_2H_6Fe_2(CO)_6$ and the hypothetical isoelectronic $O_2Fe_2(CO)_6$ molecule.

Table II. Relative Band Areas of the Transferable Ionizations of the $Fe(CO)_3$ Fragment

molecule	Fe 3d/ CO(5σ 1π)	CO(736)/ CO(584)[d]
$LFe(CO)_3$[a]	0.16	0.6
$Fe_2(CO)_6S_2$	0.16[b]	0.6
$Fe_2(CO)_6B_2H_6$	0.17[c]	0.5
$1,2\text{-}[Fe(CO)_3]_2B_3H_7$	0.16	0.6

[a] Average value for six compounds containing a single $Fe(CO)_3$. See ref 3. [b] For seven Fe IP's in band 1. [c] For seven Fe IP's and 1 B IP in bands 1 and 2. [d] Ratio of band areas (736 Å/584 Å) assigned to BH IP's assumed = 1.0.

result from the ionization of orbitals that contain large bridging ligand character and cannot be considered to be transferable from molecule to molecule. The empirical analysis of the spectra of the ferraboranes begins with the location of the transferable IP's of $Fe_2(CO)_6$ and then proceeds to the IP's associated with the borane fragment and the borane–iron interactions.

(A) $Fe_2(CO)_6B_2H_6$. The proposed structure of this ferraborane[11] is shown in Figure 2a where it is compared to a possible structure of the isoelectronic, but unknown, $Fe_2(CO)_6O_2$ molecule (Figure 2b). The latter compound is the first-row analogue of the structurally characterized $Fe_2(CO)_6S_2$ discussed above. The PE spectra of the ferraborane are shown in Figure 3, and the numerical data are given in Table I. The relative intensity changes[12] in going from He I to Ne I radiation show clearly that the transferable IP's associated with

(9) For leading references to Koopmans' theorem, see: Calabro, D. C.; Lichtenberger, D. L. *Inorg. Chem.* **1980**, *19*, 1732.
(10) Andersen, E. L.; Fehlner, T. P.; Foti, A. E.; Salahub, D. R. *J. Am. Chem. Soc.* **1980**, *102*, 7422.
(11) Andersen, E. L.; Fehlner, T. P. *J. Am. Chem. Soc.* **1978**, *100*, 4606.
(12) Relative intensity changes with photon energy reflect orbital compositions. See: Rabalais, J. W. "Principles of Ultraviolet Photoelectron Spectroscopy"; Wiley-Interscience: New York, 1977.

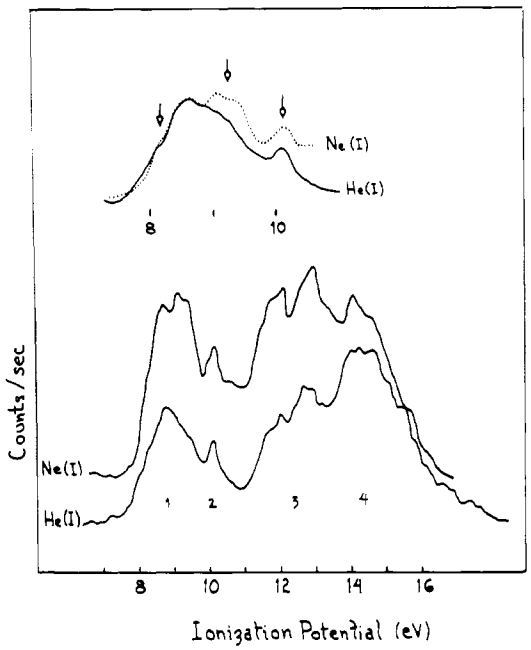

Figure 3. The He I and Ne I PE spectrum of $Fe_2(CO)_6B_2H_6$ with an expanded view of the 8–10-EV range. The first arrow points to a definite shoulder on the band onset and the next two arrows indicate the enhanced intensity of the Ne I spectrum compared to the He I spectrum.

the $Fe_2(CO)_6$ fragment are to be found in bands 1 and 2 (Fe 3d) and band 4 (CO 5σ and 1π). It is also clear from the relative intensity changes that there is at least one IP in band 1 that has large boron character. Relative areas suggest no more than two such IP's in bands 1 and 2. As the total number of IP's in the valence region should be the same as for $Fe_2(CO)_6S_2$ discussed above, this means that band 3 must contain either 4 or 3 such IP's, respectively. The relative area of band 3 suggests that the presence of 4 such IP's is more probable; hence the assignment in Table I. Although relative areas must be used with care, Table II demonstrates the internal consistency of the band areas for the transferable IP's of the $Fe(CO)_3$ fragment in compounds containing one and two iron atoms. In a strictly empirical sense, one cannot proceed further with the assignment; however, with use of model compounds, a more detailed understanding of the borane and borane–metal interaction bands may be achieved.

In the model compound approach two simple guides based on the relative effects of nuclear charge and protonation allow the ligand and ligand–metal bands of $Fe_2(CO)_6S_2$ and $Fe_2(CO)_6B_2H_6$ to be related. Reduction of nuclear charge reduces the IP of orbitals affected whereas protonation increases the IP. In going from $Fe_2(CO)_6O_2$ (i.e., $Fe_2(CO)_6S_2$) to $Fe_2(CO)_6B_2H_6$, three protons are formally removed from each oxygen nucleus, two being placed in bridging position and one in a terminal position. The amount of stabilization can only be guessed insofar as both nuclear charge and protonation effects are spread over a number of orbitals. On the other hand, using the C_2H_4/B_2H_6 pair[13] as a guide yields the estimated IP's of $Fe_2(CO)_6B_2H_6$ shown in Figure 4a. To obtain the estimated IP's, we used the observed PE bands for $Fe_2(CO)_6S_2$, a destabilization of 1.0 eV per unit nuclear charge, and a stabilization of 1.8 eV for protonation. The model approach predicts one IP of high boron character in the Fe 3d band and 4 IP's at higher ionization energy.

With one significant exception, a similar result is obtained in a comparison of the Fenske–Hall eigenvalues of the same

(13) Brundle, C. R.; Robin, M. B.; Basch, H.; Pinsky, M.; Bond, A. *J. Am. Chem. Soc.* **1970**, *92*, 3863.

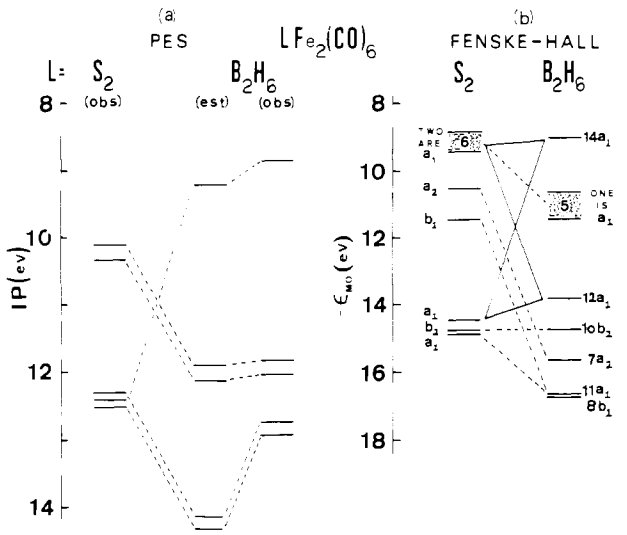

Figure 4. Correlation diagram for $LFe_2(CO)_6$ where L = S_2 and B_2H_6: (a) according to PES ("est" refers to model approach described in text) (note that the Fe(3d) bands are not included here); (b) according to the Fenske–Hall calculations. Note that the HOMO is not included here. The groups of orbitals labeled "6" and "5" are predominantly Fe(3d).

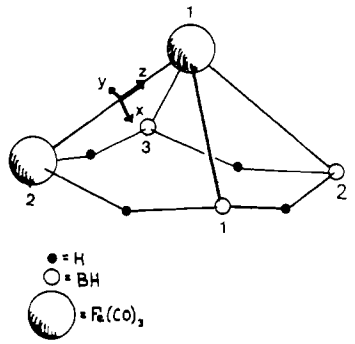

Figure 5. Schematic structure for 1,2-$[Fe(CO)_3]_2B_3H_7$. The y axis is parallel to the axis passing through B_1 and B_3.

orbitals for the two compounds (Figure 4b). The correlation shows that one MO of high boron character ($14a_1$) should occur at low IP and that the four Fe–H–B bridging MO's ($8b_1$, $11a_1$, $7a_2$, and $10b_2$) are all stabilized although the relative amounts of stabilization are, as expected, quite different. The one complicating factor in this scheme lies in the fact that there are two a_1 orbitals ($12a_1$ and $14a_1$) that contain almost equal percent character from Fe and B. The earlier empirical analysis would assign ionization from both orbitals to bands 1 and 2. On the basis of a Koopmans' theorem approach to the calculations, ionization from the lower lying MB orbital ($12a_1$) could be assigned to either band 2 (mainly metal MO's) or to band 3 (mainly boron MO's). The relative intensity measurements as a function of photon energy strongly suggest the former assignment.

Two aspects of the assigned distribution of radical cation states for the ferraborane deserve comment. First, the spectra imply that the $14a_1$ orbital with significant B–B character lies at low binding energy and may well exhibit reactivity similar to B–B bonds in B_6H_{10} or $B_5H_8^-$. Second, the fact that the $7a_2$ and $8b_1$ M–B bridging orbitals are substantially stabilized in the ferraborane requires a reduction in Fe 3d character with respect to the analogous orbitals in $Fe_2(CO)_6S_2$. This suggests greater $Fe_2(CO)_6^{\delta+}B_2H_6^{\delta-}$ charge separation than $Fe_2(CO)_6^{\delta+}S_2^{\delta-}$ charge separation. Indeed, the charge separation is 1.16 for $Fe_2(CO)_6B_2H_6$ vs. 0.07 for $Fe_2(CO)_6S_2$ as calculated by the Fenske–Hall method. The negative nature of the B_2H_6

Table III. Vertical Ionization Potentials, Relative Band Areas, Band Character, and Calculated Eigenvalues[a] for 1,2-$[Fe(CO)_3]_2B_3H_7$

band[b]	IP,[c] eV	A/E[d] (rel)	$A/E(736)/A/E(584)$[e]	IP's[f] per band	band character[f]	F–H eigenvalues, eV	EHT eigenvalues, eV	
1	8.5, 9.0	0.2	0.6	6	Fe(3d)	29a′, 3.40, LUMO	9.11	
						28a′, 8.47, HOMO, Fe_1, Fe_2(3d)	11.94	Fe(3d)
						18a″, 9.32, Fe_1(3d)	11.96	
						27a′, 9.59, Fe_1(3d)	12.12	
						26a′, 10.41, Fe_1, Fe_2(3d)	12.30	
						17a″, 10.50, Fe_1, Fe_2(3d), B(2p)	12.36	
						25a′, 11.36, Fe_2(3d)	12.37	
2	9.4, 10.0	0.1	1.2	3	Fe(3d), B(2p)	24a′, 11.94, Fe_1, Fe_2(3d), B(2p)	11.17	Fe–B
						16a″, 12.45, Fe_1, Fe_2(3d), B(2p)	11.22	
						23a′, 13.88, Fe_1, Fe_2(3d), B(2p)	11.66	
3	11.4, 11.8, 13.1	0.4	[1.0]	4	B(2p), H(1s)	22a′, 16.62, H_b–B–H_t	13.43	H_b–B–H_t
						15a″, 17.16, CO, 5σ	13.59	
						14a″, 17.31, BH_t	14.02	
						21a′, 17.49, CO, 5σ	14.03	
						20a′, 18.50, BH_t		
						13a″, 18.52, BH_t		
4	14.6	1.0	0.6	18	CO(5σ, 1π)	19–22.5[g], CO(5σ, 1π)	14.1–15.7, CO	

[a] The signs of all eigenvalues have been changed from negative to positive for ease of comparison with IP's via Koopmans' theorem. [b] See Figure 6. [c] Vertical IP's; sh = shoulder. [d] He I band area over mean electron energy. [e] [] defined as 1.0. [f] According to assignment described in text. [g] In the range of 19–22.5 eV there are 19 eigenvalues; three of these have significant B–H character.

fragment is discussed further below.

(B) 1,2-$[Fe(CO)_3]_2B_2H_7$. The solid-state structure[6] of this ferraborane is shown in Figure 5. Although this compound contains the formal analogue of the allyl ligand ($C_3H_5^-$), there is in fact no structural relationship. However, the $Fe_2(CO)_6$ fragment is structurally very similar to that found in the two compounds discussed above. For this reason, the PE spectra of this compound can be approached in the same manner as for $Fe_2(CO)_6B_2H_6$.

The PE spectra of this ferraborane are shown in Figure 6, and the numerical data are gathered in Table III. The relative intensity changes in going from He I to Ne I radiation show that the transferable IP's associated with the $Fe_2(CO)_6$ fragment are to be found in bands 1 (Fe 3d) and 4 (CO 5σ and 1π). Note that there is no shoulder on the low-IP edge of band 1 and that the relative areas suggest only 6 IP's in band 1. Since both $Fe_2(CO)_6S_2$ and $Fe_2(CO)_6B_2H_6$ exhibit a shoulder which is assigned to an a_1 (Fe–Fe) ionization, the data here suggest that one of the Fe(3d) IP's for $Fe_2(CO)_6B_3H_7$ lies at higher IP, i.e., band 2. Band 2 contains other IP's with substantial iron character, and these may be associated with borane–iron interaction orbitals. By difference, band 3 contains the IP's associated mainly with the B_3H_7 fragment.

To proceed beyond this gross assignment, it is necessary to count orbitals as well as to develop simple descriptions of the orbitals in terms of atomic character. In going from $Fe_2(CO)_6B_2H_6$ to $Fe_2(CO)_6B_3H_7$, four valence electrons are added and, thus, two additional filled orbitals. It is clear that one of the two added orbitals will contain significant B(2s)–H(1s) character and hence lie at high ionization energy (17–22 eV). The second added orbital will contain significant boron 2p character, and consequently this orbital will involve some combination of Fe/B/H bonding placing it at lower ionization energy (band 2 or 3). On the basis of calculated Fenske-Hall eigenvalues (Table III), it is not possible to state clearly where this second added orbital will lie. The assignment in Table III places the second added orbital in band 2 which is consistent with but not required by the relative area measurements. The complete assignment is given in Table III.

Two comments result from a consideration of the assigned spectra. First, band 1 (Fe 3d) is split, suggesting the geometrically different iron atoms have significantly different charges. Second, there are nine IP's with large Fe 3d character rather than the eight found for $Fe_2(CO)_6B_2H_6$, suggesting less positive charge for the $Fe_2(CO)_6$ fragment in $Fe_2(CO)_6B_3H_7$ compared to that in $Fe_2(CO)_6B_2H_6$.

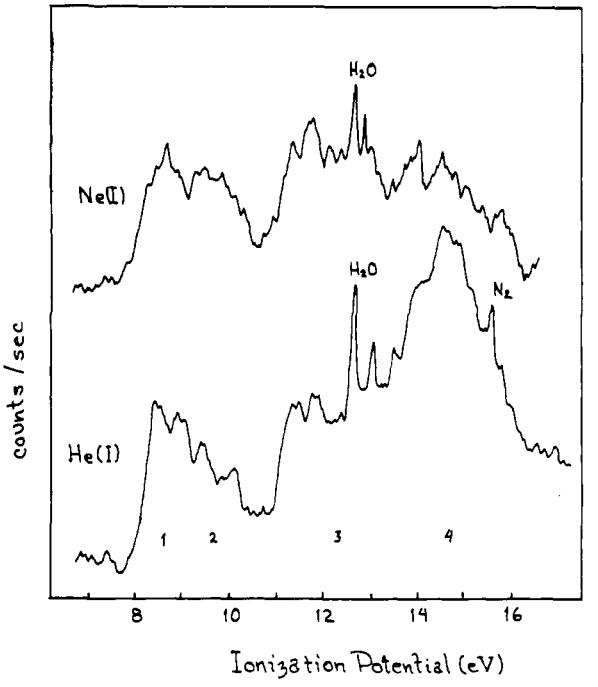

Figure 6. He I and Ne I PE spectra of 1,2-$[Fe_2(CO)_3]_2B_3H_7$.

The assigned spectra also allow examination of the borane analogy as a function of metal cage content in terms of the measured distribution of radical cations states. This is shown in Figure 7 for B_5H_9,[14] 1-$Fe(CO)_3B_4H_8$,[3] and 1,2-$[Fe(CO)_3]_2B_3H_7$. As more and more metal atoms are added to the system, there is a gradual shift in the states associated with cluster bonding towards lower ionization potential. In terms of counting orbitals, the borane analogy holds for the two metal derivatives, but in terms of predicting ionization energies, the analogy is only useful in an approximate sense for the monoiron compound.

(II) Electronic Structure. As our interest lies in understanding the basic electronic structure of these diiron systems, we wish to go beyond the simple assignment and rationalization of the distribution of radical cation states as observed by UV–photoelectron spectroscopy. In this exploration of the

(14) Lloyd, D. R.; Lynaugh, N.; Roberts, P. J.; Guest, M. F. *J. Chem. Soc., Faraday Trans. 2*, **1975**, *71*, 1382.

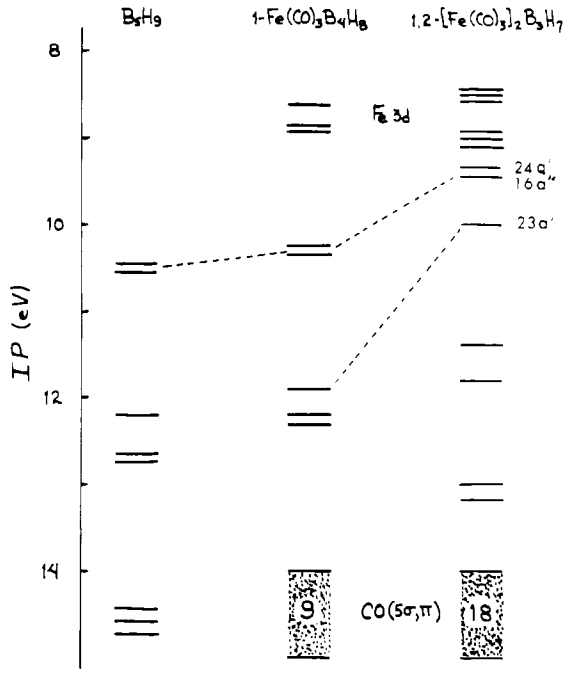

Figure 7. Correlation diagram for the radical cation states observed in the PE spectra of B_5H_9, 1-$Fe(CO)_3B_4H_8$, and 1,2-$[Fe(CO)_3]B_3H_7$.

bonding of these diiron ferraboranes, we have used the extended Hückel[7] and Fenske–Hall[8] quantum chemical methods. A quantitative comparison of the extended Hückel and Fenske–Hall eigenvalues with the PE spectra with use of Koopmans' theorem has already been given in Tables I and III. Looking first at the extended Hückel eigenvalues, we find the transferable Fe(3d) MO's are out of order in terms of the IP's for 1,2-$[Fe(CO)_3]_2B_3H_7$. Otherwise, a 1–2-eV shift yields nearly quantitative agreement with the PE spectra for both compounds. The order of Fenske–Hall eigenvalues is in good agreement with the assigned PE spectra, although the eigenvalues are spread over a much wider energy range than observed experimentally. We also note that the Fenske–Hall calculations on 1,2-$[Fe(CO)_3]_2B_3H_7$ place some of the CO 5σ-type orbitals in the 16.5–18.5-eV range, along with BH-type orbitals. We feel that this is an artifact of the calculations; BH-type orbitals are calculated to be much too stable relative to the CO 5σ orbital in B_5H_9 and CO.[15]

As both the extended Hückel and Fenske–Hall methods have proven useful in discussing qualitative bonding interactions, we use them here to examine a number of interesting physical properties of these diiron ferraborane cages in terms of the borane analogy defined above.

(A) Cluster Bonding in 1,2-$[Fe(CO)_3]_2B_3H_7$. A Mulliken overlap population analysis on the nine uppermost MO's reveals that the top six are mainly Fe(3d) in character. Of these six, only the HOMO (28a′) has any significant Fe–Fe bonding character and only the 17a″ MO contains significant iron–boron bonding (Fe_1 with B_1 and B_3). These top six MO's can be classified as predominantly nonbonding in the five-atom nido cage.

The orbitals that contribute most to the cluster bonding are the next three MO's (23a′, 16a″, 24a′). In Figure 8 schematic drawings of these three orbitals are shown. These are derived from the Fenske–Hall calculations and correspond to the indicated ionizations in Figure 7. In terms of orbitals, the borane analogy holds well as seen by comparing the orbital sketches with those of the corresponding cluster orbitals in B_5H_9 (Figure 8). The difference is simply that in the diiron ferraborane the cluster orbitals utilize Fe 3d AO's in place of B 2p AO's.

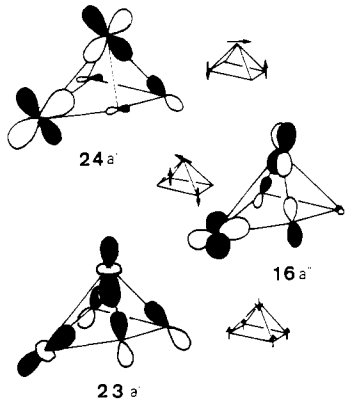

Figure 8. Schematic diagrams for the 23a′, 16a″, and 24a′ molecular orbitals of 1,2-$[Fe(CO)_3]_2B_3H_7$. The predominant character of the corresponding three cluster molecular orbitals of B_5H_9 is also shown.

(B) Charge Distributions. The basic question explored in this section is whether the distribution of charge over the cluster atoms is primarily due to cage geometry or cage composition. The five atom nido cage is ideal for seeking an answer to this question as it is well established both experimentally and theoretically for B_5H_9 that the apical boron atom is significantly more negative than the four basal atoms. The experimental evidence consists of dipole moment measurements,[16] relative ^{11}B chemical shifts,[17] position of electrophilic substitution,[18] and analysis of cage substituent effects probed by photoelectron spectroscopy.[19] Both crude and sophisticated MO treatments give the same charge distribution and, in addition, provide an explanation in terms of the orbitals of the system.[20] In essence, the greater negative charge on the apical boron results from the fact that the geometrical position of this boron in the cage requires a greater utilization of the 2p atomic orbitals in the framework molecular orbitals relative to a basal boron; i.e., because the B 2p orbitals are not fully utilized in any electron dificient cage,[21] the greater the utilization in a particular cage position, the greater the relative negative charge at that position. The question posed then is whether the relative charge distribution of this five-atom nido cage remains qualitatively the same if boron is replaced by transition-metal atoms. A compound available for testing this question is 1,2-$[Fe(CO)_3]_2B_3H_7$ as it has one apical and one basal iron atom.

There are three experimental indications of the relative charges of the apical and basal iron atoms in $Fe_2(CO)_6B_3H_7$. First, the photoelectron spectrum (see above) exhibits an Fe 3d band that is split by 0.5 eV. This fact, coupled with the knowledge that Fe 3d IP's increase by 10–15 eV for each unit increase in positive charge,[22] suggests a relative charge difference of about 5%, i.e., there is a significant difference in charge between the two iron atoms. Second, a comparison of the CO stretching regions in the infrared shows that there is a qualitative difference in the CO absorption pattern for

(15) The first IP of CO is calculated to be 13.8 eV compared to an experimental value of 14.0 eV. The corresponding values for B_5H_9 are 15.5 and 10.5 eV.

(16) Hrostowski, H. J.; Meyers, R. J.; Pimentel, G. C. *J. Chem. Phys.* **1952**, *20*, 518.
(17) Lipscomb, W. N.; Eaton, G. R. "NMR Studies of Boron Hydrides and Related Compouds"; W. A. Benjamin: New York, 1969.
(18) Shore, S. G. In "Boron Hydride Chemistry"; Muetterties, E. L., Ed.; Academic Press: New York, 1975.
(19) Ulman, J. A.; Fehlner, T. P. *J. Am. Chem. Soc.* **1976**, *98*, 1119.
(20) Switkes, E.; Epstein, I. R.; Tossell, J. A.; Stevens, R. M.; Lipscomb, W. N. *J. Am. Chem. Soc.* **1970**, *92*, 3837.
(21) Andersen, E. L.; DeKock, R. L.; Fehlner, T. P. *J. Am. Chem. Soc.* **1980**, *102*, 2644.
(22) Ballhausen, C. J.; Gray, H. B. "Molecular Orbital Theory"; W. A., Benjamin: Menlo Park, CA, 1965; p 120.

Table IV. ^{11}B NMR Data for $Fe_2(CO)_6B_2H_6$ and $1,2\text{-}[Fe(CO)_3]_2B_3H_7$

	$^{11}B\{^1H\}$[a]	$J_{^{11}B-H}$, Hz
$Fe_2(CO)_6B_2H_6$	−24	~60
$1,2\text{-}[Fe(CO)_3]_2B_3H_7$	4.2 ($B_{1,3}$)	160
	12.1 (B_2)	170

[a] In ppm; positive, downfield from $BF_3 \cdot O(C_2H_5)_2$.

Table V. Mulliken Charges for $Fe_2(CO)_6B_2H_6$ and $1,2\text{-}[Fe(CO)_3]_2B_3H_7$

atom	EHT	F-H	atom	EHT	F-H
		$Fe_2(CO)_6B_2H_6$			
Fe	1.20	0.46	H_t	−0.24	−0.003
C_{av}	0.57	0.06	H_b	−0.19	−0.08
O_{av}	−0.78	−0.02	B_2H_6	−1.14	−1.19
B	0.05	−0.43			
		$1,2\text{-}[Fe(CO)_3]_2B_3H_7$			
Fe_1	0.65	0.30	$B_{1,3}$	0.43	−0.39
Fe_2	1.19	0.44	B_2	0.44	−0.12
C_{1av}	0.45	0.13	H_t	−0.26	−0.03
O_{1av}	−0.84	−0.08	$H_{b,BFe}$	−0.20	−0.07
C_{2av}	0.59	0.11	$H_{b,BB}$	−0.13	0.13
O_{2av}	−0.78	−0.01	B_3H_7	−0.14	−0.87

$Fe_2(CO)_6B_3H_7$[6] compared to that for $Fe_2(CO)_6S_2$[23] and $Fe_2(CO)_6B_2H_6$.[24] The lowest frequencies of significant intensity for each compound are 1955, 2005, and 2003 cm^{-1}, respectively. This suggests that the negative charge on the CO's of one $Fe(CO)_3$ group of $Fe_2(CO)_6B_3H_7$ is greater than that on the CO's of either $Fe_2(CO)_6S_2$ or $Fe_2(CO)_6B_2H_6$. In turn, this implies one of the iron atoms of the first compound is more negative than the iron atoms of the other two. The third source of information is the ^{11}B chemical shifts and B–H coupling constants. These are compiled in Table IV for the two ferraboranes. Both the absolute chemical shifts as well as the large chemical shift difference between the boron resonances of the two ferraboranes strongly suggest a significant difference in boron charge, the B_2H_6 compound being more negative than the B_3H_7 compound. The relatively small J_{BH} for $Fe_2(CO)_6B_2H_6$ and the "normal" (for neutral boranes) J_{BH} for $Fe_2(CO)_6B_3H_7$ are consistent with the chemical shift.[17] Thus, the NMR data imply a greater net negative charge on the $Fe_2(CO)_6$ fragment in $Fe(CO)_6B_3H_7$ than in $Fe_2(CO)_6B_2H_6$.

The charge distributions have also been explored with the use of the extended Hückel and Fenske–Hall methods and a Mulliken charge analysis. The calculated atom changes as well as sums from various fragments are shown in Table V as obtained by both methods. Although the absolute charges calculated by the two methods are significantly different, the calculated trends are the same. In either case the iron atoms in $Fe_2(CO)_6B_2H_6$ are predicted to have approximately the same charge as the basal iron atom in $Fe_2(CO)_6B_3H_7$. Also, both methods predict the apical iron atom to be less positive than the basal iron atom in $Fe_2(CO)_6B_3H_7$. Notice too that in both calculations the CO's associated with the apical iron of this compound carry more electronic charge than those associated with the basal iron. Finally, similar charge trends are predicted by the calculations for the boron and hydrogen atoms and for the B_2H_6 moiety compared to the B_3H_7 moiety. There is more electronic charge associated with the boron atoms in B_2H_6 than either type of boron atom in the B_3H_7 fragment. All of these trends and differences are in agreement with the experimental information presented above concerning relative charges on Fe, CO, and B.

Table VI. Percent Contribution[a] of Fe 3d AO's to the Upper Nine MO's of $1,2\text{-}[Fe(CO)_3]_2B_3H_7$

MO	% 3d Fe_1	% 3d Fe_2	MO	% 3d Fe_1	% 3d Fe_2
28a′	21	18	25a′	3	76
18a″	56	1	24a′	23	48
27a′	69	5	16a″	18	43
26a′	41	21	23a′	12	7
17a″	26	35			

[a] From Fenske–Hall calculations.

We now turn our attention explicitly to the difference in charge between the apical and basal iron atoms in $Fe_2(CO)_6B_3H_7$. The conclusion is the same whether we employ extended Hückel or Fenske–Hall calculations: there is more valence atomic orbital involvement by the apical Fe atom than by the basal Fe atom. In the former calculation it is the $3d_{xy}$ orbital (see coordinate system, Figure 5) that becomes more involved and in the latter the $4p_y$ orbital. In the C_s symmetry of this complex, $3d_{xy}$ and $4p_y$ have the same symmetry (a″). Like BH, the $Fe(CO)_3$ fragment behaves as an orbital-rich (or electron-poor) species and when placed in the apical position is forced to utilize more orbitals in cage bonding than when placed in a basal position. Thus, in clusters containing orbital-rich atoms, the distribution of charge is significantly affected by the bonding requirements of the cage position as well as by the identity of the atom. That this statement holds for a transition metal as well as boron is particularly significant.

The charge difference between the apical and basal Fe atoms also becomes apparent upon examination of the % 3d contribution to each of the upper nine occupied MO's. These results are shown in Table VI and illustrate that the less positive Fe atom (Fe_1) contributes more 3d character to the less stable MO's whereas the more positive Fe atom (Fe_2) contributes more 3d character to the more stable MO's.

(C) UV–Visible Absorptions. As has been pointed out above, in terms of properties related to geometry and cluster bonding, the borane analogy is quite useful in understanding the nature of $1,2\text{-}[Fe(CO)_3]_2B_3H_7$. There is, however, one aspect of the electronic structure of metallaboranes that has no counterpart at all in pure boranes. This results from the fact that the metallaboranes have high-lying filled metal d orbitals and, presumably, low-lying unfilled metal d orbitals. Thus, these compounds invariably absorb in the UV–visbile region and studies of $1\text{-}Fe(CO)_3B_4H_8$ illustrate the fact that these compounds also undergo some interesting and useful photochemistry.[4] The discussion of the absorption properties of the diiron ferraboranes that follows is qualitative in nature but does reveal some aspects of the lowest unoccupied MO of these compounds.

The measured solution spectra of the two diiron ferraboranes are shown in Figure 9, and the data are compared with those of related compounds in Table VII. The spectra of the diiron ferraboranes are qualitatively different from those of monoiron derivatives in that a greater number of distinct bands are observed. The spectra are qualitatively similar to that for $Fe_2(CO)_6S_2$ which is evidence that the absorption properties of these compounds reflect the $Fe_2(CO)_6$ fragment perturbed by the borane "ligand".

Neither sufficient data nor theory exists to assign these spectra with confidence; however, some indication of the nature of the absorptions may be gained through analogy to other compounds containing two adjacent metal atoms. Perhaps the most completely studied compound of this type is $Mn_2(CO)_{10}$, a compound that contains a Mn–Mn bond.[25] The two lowest

(23) Hieber, W.; Gruber, I. *Z. Anorg. Allg. Chem.* **1958**, *296*, 91.
(24) Andersen, E. L.; Fehlner, T. P. *J. Am. Chem. Soc.* **1978**, *100*, 4606.
(25) Levenson, R. A.; Gray, H. B. *J. Am. Chem. Soc.* **1975**, *97*, 6042.

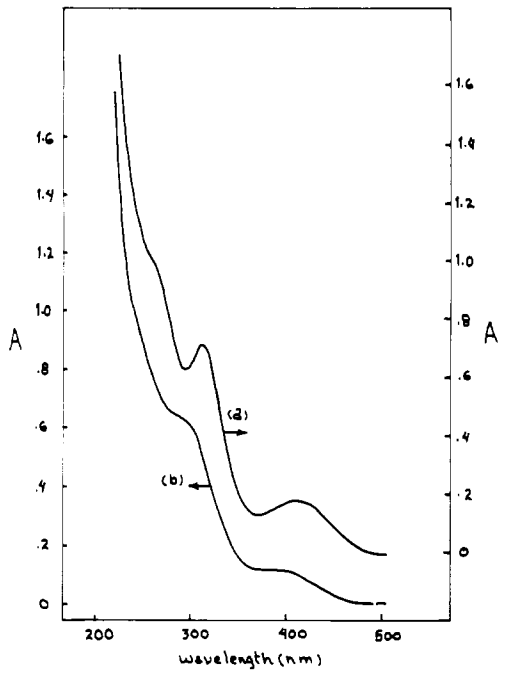

Figure 9. The UV-visible spectra of (a) $Fe_2(CO)_6B_2H_6$ and (b) 1,2-$[Fe(CO)_3]_2B_3H_7$.

Table VII. UV-Visible Absorption Bands and Calculated Properties of Diiron Ferraboranes and Related Compounds

	abs peaks,[a] eV	extinctn coeff	ΔE_{calcd} ($\sigma \rightarrow \sigma^*$)[c], eV		Fe-Fe Mulliken OP[b]	
			EHT	F-H	EHT	F-H
1,2-$[Fe(CO)_3]_2B_3H_7$[b]	3.22					
	4.36	$\sim 10^3$	2.11	5.07	0.03	0.15
$Fe_2(CO)_6B_2H_6$[b]	3.03					
	4.01	$\sim 10^3$	1.92	4.84	0.00	0.18
	4.83 sh					
$Fe_2(CO)_6S_2$[c]	2.72	$\sim 10^3$				
	3.73	1.2×10^4	1.84	4.03	−0.03	0.11
	4.55 sh					
$Mn_2(CO)_{10}$[d]	3.31	2.9×10^3				
	3.69	3.4×10^4				

[a] sh = shoulder. [b] Measured at 25 °C in pentane. [c] Reference 23. [d] Reference 25. [e] Difference in appropriate orbital energies. [f] Mulliken overlap population.

energy absorptions are given in Table VII and are assigned in terms of MO's to: 3.31 (Mn 3d "nonbonding" to MnMn antibonding ($d\pi \rightarrow \sigma^*$)) and 3.69 eV (MnMn bonding to MnMn antibonding ($\sigma \rightarrow \sigma^*$)). The prominent characteristics of the latter absorption are a large extinction coefficient and a large temperature dependence of the absorption maximum. By analogy, the lowest energy absorption in the diiron ferraboranes is assigned to a $d\pi \rightarrow \sigma^*$ transition and the absorption next higher in energy having a larger extinction coefficient to the $\sigma \rightarrow \sigma^*$ transition.

Focusing our attention on the most intense bands, the approximate calculations on the diiron ferraboranes support its assignment to a $\sigma \rightarrow \sigma^*$ transition. First, the Fenske–Hall calculations predict the HOMO to have a FeFe σ-bonding character and the LUMO to be Fe–Fe σ antibonding. Second, the $\sigma \rightarrow \sigma^*$ energy difference does correlate with the blue shifts in the two lowest absorptions as one goes from $Fe(CO)_6S_2$ to $Fe_2(CO)_6B_2H_6$ to $Fe_2(CO)_6B_3H_7$ (Table VII). This suggests an increased metal–metal interaction in the diiron ferraboranes compared to $Fe_2(CO)_6S_2$, a suggestion that is supported by the net Fe–Fe Mulliken overlap populations (Table VII). It is well-known that bridging ligands affect metal–metal interactions, and it now appears that boranes acting as "bridging ligands" enhance the strength of the metal–metal interaction.

(D) Fluxional Properties of 1,2-$[Fe(CO)_3]_2B_3H_7$. Although the similarity in geometry of this compound to B_5H_9 has been noted in conjunction with the borane analogy, there are significant differences in structural properties as well. A particularly interesting difference is the fact that although the three hydrogen atoms attached to B_2 (see Figure 5) are inequivalent in the solid state, in solution they are found to be magnetically equivalent. Hence this portion of the molecule is fluxional in that two BHB bridging hydrogens and one BH terminal hydrogen are interconverted rapidly on the NMR time scale. Similar behavior is not observed for B_5H_9.

Although there is no necessary connection with the fluxional behavior of the ferraborane, we have observed that the total Mulliken overlap population for Fe_1–B_2 is significantly less than for Fe_1–$B_{1,3}$ in both the Fenske–Hall and the extended Hückel calculations. The results are 0.006 vs. 0.22 for the Fenske–Hall calculations and −0.03 vs. 0.09 for the extended Hückel calculations. This difference in bonding is also suggested by simple valence bond considerations. With the Fe–Fe bond considered as localized, the structure for B_5H_9 (I) has

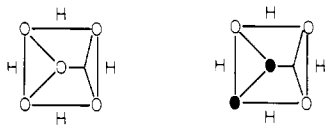

B_5H_9
I, ○ = BH

1,2-$[Fe(CO)_3]_2B_3H_7$
II, ○ = BH, ● = $Fe(CO)_3$

three more resonance forms while that for the ferraborane has only one more. The net result is that the Fe_1–B_2 bond order is less than the Fe_1–$B_{1,3}$ bond orders. The relationship of this differential bonding of the three boron atoms to the fluxional behavior is not obvious as the mechanism for the latter is not known. But both the dynamic behavior of the ferraborane and the specific bonding difference with respect to the related borane emphasizes the fact that significant and important structural and bonding differences appear when iron atoms replace boron atoms in a cage.

Experimental Section

The samples of diiron ferraboranes used in this work were prepared as described elsewhere.[6,24] Each sample was characterized by ^{11}B and ^1H NMR. Mass spectrometric analysis of the vapor above the liquid or solid samples at room temperature showed that the vapor was composed of $Fe_2(CO)_6B_2H_6$ and $Fe_2(CO)_6B_3H_7$, respectively. Photoelectron spectra were recorded at room temperature with use of He I (21.2 eV) and Ne I (16.8 eV) radiation. The spectrometer[26] was operated at a resolution of 20 meV (fwhm) at 5 eV for $Fe_2(CO)_6B_2H_6$ and 35 meV at 5 eV for $Fe_2(CO)_6B_3H_7$. An internal calibrant of xenon and argon was used. The UV-visible spectra were measured on a Cary 15 spectrophotometer. The solvent, pentane, was distilled in vacuo at room temperature from lithium aluminum hydride immediately prior to use.

Calculations. Molecular Geometry. Both the extended Hückel and Fenske–Hall quantum chemical calculations were carried out on the two ferraboranes. The sawhorse geometry of the $Fe_2(CO)_6$ fragment was chosen to be the same in both molecules. Its structure was idealized to C_{2v} symmetry with bond angles taken from the structure of $Fe_2(CO)_6S_2$.[27] The pertinent angles are $C_1Fe_1C_2 = C_4Fe_2C_6 = 94°$, $C_3Fe_1Fe_2 = C_5Fe_2Fe_1 = 155°$, and $C_4Fe_2Fe_1 = C_6Fe_2Fe_1 = C_1Fe_1Fe_2 = C_2Fe_1Fe_2 = 98°$. Bond lengths in the $Fe_2(CO)_6$ fragment were chosen the same as those adopted by Teo et al.[28] in their Fenske–Hall calculations on $Fe_2(CO)_6X_2$ molecules. These are Fe–Fe

(26) Fehlner, T. P. *Inorg. Chem.* **1975**, *14*, 934.
(27) Wei, C. H.; Dahl, L. F. *Inorg. Chem.* **1965**, *4*, 1.
(28) Teo, B. K.; Hall, M. B.; Fenske, R. F.; Dahl, L. F. *Inorg. Chem.* **1975**, *14*, 3103.

= 2.55 Å, C-O = 1.15 Å, and Fe-C = 1.78 Å.

The geometry of $Fe_2(CO)_6B_2H_6$ was idealized to C_{2v} symmetry as shown in Figure 2. All BBH angles were chosen to be 110° with bond lengths of B-H_t = 1.05 Å, B-H_b = 1.30 Å, B-B = 1.70 Å, Fe-H_b = 1.55 Å, and Fe-B = 2.22 Å. The geometry of the B_3H_7 fragment on $Fe_2(CO)_6$ was based on the crystal structure study,[6] with slight adjustments in positions of the B and H atoms in order to idealize C_s symmetry.

Basis Functions. The extended Hückel calculations employed the same orbital exponents and diagonal matrix elements for Fe, C, and O as used by Burdett.[29] For boron and sulfur we employed Slater exponents for the valence orbitals; 1.3 and 1.82, respectively. The H 1s orbital exponent was chosen to be 1.3 and its diagonal matrix -13.60 eV. The diagonal matrix elements for boron and sulfur were chosen from the work of Basch, Viste, and Gray.[30] The extended Hückel calculations were done employing the arithmetric mean Wolfsberg-Helmholz approximation with K = 1.75.

The Fenske-Hall calculations employed single-ζ Slater basis functions for the 1s and 2s functions of B, C, and O. The exponents were obtained by curve fitting the double-ζ functions of Clementi[31] while maintaining orthogonal functions. For hydrogen, an exponent of 1.16 was used which corresponds to the minimum energy exponent for methane.[32] The sulfur functions were used directly in their double-ζ form.[33] The iron 1s-3d functions were taken from the results of Richardson et al.[34] and were all single-ζ except the 3d function which is double-ζ and was chosen for the +1 oxidation state of iron. The 4s and 4p exponents were both chosen to be 2.0. For all of the atoms studied here, these are the basis functions typically employed by Fenske and Hall in their studies using this quantum chemical approach.[8,35,36]

Acknowledgment. The support of the National Science Foundation under Grants CHE 78-11600 and CHE 79-15220 is gratefully acknowledged. We thank the University of Notre Dame and the Calvin College Computer Centers for providing computing time.

Registry No. $Fe_2(CO)_6B_2H_6$, 67517-57-1; 1,2-$[Fe(CO)_3]_2B_3H_7$, 71271-99-3; $Fe_2(CO)_6S_2$, 14243-23-3.

(29) Burdett, J. K. *J. Chem. Soc., Dalton Trans.* **1977**, 424.
(30) Basch, H.; Viste, A.; Gray, H. B. *Theor. Chim. Acta* **1964**, *3*, 458.
(31) Clementi, E. *J. Chem. Phys.* **1964**, *40*, 1944.
(32) Hehre, W. J.; Stewart, R. F.; Pople, J. A. *J. Chem. Phys.* **1969**, *51*, 2657.
(33) Clementi, E. *IBM J. Res. Dev.* **1965**, *9*, 2.
(34) Richardson, J. W.; Nieuwpoort, W. C.; Powell, R. R.; Egell, W. F. *J. Chem. Phys.* **1962**, *36*, 1057.
(35) Sherwood, Jr., D. E.; Hall, M. B. *Inorg. Chem.* **1980**, *19*, 1805.
(36) A recent report includes some results of an extended Hückel calculation on 1,2-$[Fe(CO)_3]_2B_3H_7$: Bint, R. P.; Pelin, K.; Spalding, T. R. *Inorg. Nucl. Chem. Lett.* **1980**, *16*, 391.

Contribution from the Department of Chemistry, University of Cincinnati, Cincinnati, Ohio 45221

Technetium Electrochemistry. 1. Spectroelectrochemical Studies of Halogen, diars, and diphos Complexes of Technetium in Nonaqueous Media

ROGER W. HURST, WILLIAM R. HEINEMAN, and EDWARD DEUTSCH*

Received March 3, 1981

Spectroelectrochemical techniques have been used to investigate the electrochemistry of the well-characterized trans-octahedral Tc(III) complexes $[TcD_2X_2]^+$ where D = diars (*o*-phenylenebis(dimethylarsine)) or diphos (1,2-bis(diphenylphosphino)ethane) and X = Cl, or Br, or I. All complexes exhibit reversible Tc(III)/Tc(II) couples, and the diars complexes exhibit less well-characterized Tc(II)/Tc(I) couples. For the complex $[Tc(diars)_2Cl_2]^+$ in *N*,*N*-dimethylformamide with 0.5 M tetraethylammonium perchlorate as supporting electrolyte, reduction potentials for the Tc(III)/Tc(II) and Tc(II)/Tc(I) couples are -0.091 and -1.29 V vs. NaSCE, respectively. The potential of the Tc(III)/Tc(II) couple is sensitive to the nature of D and to the nature of X, varying Cl → Br, Br → I, or diars → diphos, favoring reduction to Tc(II) by 70-120 mV. These Tc(III)/Tc(II) couples are biologically accessible, and the sensitivity of reduction potential to the nature of X may be one source of the biological differentiation among $[^{99m}Tc(diars)_2X_2]^+$ complexes. Comparisons with literature data show that, independent of oxidation state, technetium complexes are 200-300 mV more easily reduced than are the corresponding rhenium complexes. Observations on the reduction of the Tc(IV) complexes TcX_6^{2-}, X = Cl or Br, and comments on the lability of Tc-X bonds are also presented.

Introduction

The chemistry of technetium is currently receiving considerable attention[1-9] primarily because of the preeminence of ^{99m}Tc in diagnostic nuclear medicine[1,10] but also because of the paucity of information currently available about this element which occupies a central position among the d-block metals. Technetium electrochemistry is especially poorly developed, despite the fact that complexes are known in which technetium exhibits oxidation states ranging from VII to -I.[11,12] This situation arises since almost all the tecnetium complexes available until very recently undergo only irreversible electrochemical behavior,[13] making it difficult to generate quantitative conclusions and comparisons. For example, Davison and co-workers[14] recently reported that the hexahalo-

(1) Deutsch, E. "Radiopharmaceuticals II"; Society of Nuclear Medicine Publishers: New York, 1979; pp 129-146.
(2) Deutsch, E.; Barnett, B. L. "Inorganic Chemistry in Biology and Medicine"; Martell, A. E., Ed.; American Chemical Society: Washington, D. C., 1980; ACS Symp. Ser. No. 140, pp 103-119.
(3) Thomas, R. W.; Davison, A.; Trop, H. S.; Deutsch, E. *Inorg. Chem.* **1980**, *19*, 2840-2842.
(4) Thomas, R. W.; Estes, G. W.; Elder, R. C.; Deutsch, E. *J. Am. Chem. Soc.* **1979**, *101*, 4581-4585.
(5) Glavan, K. A.; Whittle, R.; Johnson, J. F.; Elder, R. C.; Deutsch, E. *J. Am. Chem. Soc.* **1980**, *102*, 2103-2104.
(6) Libson, K.; Deutsch, E.; Barnett, B. L. *J. Am. Chem. Soc.* **1980**, *102*, 2476-2478.
(7) Trop, H. S.; Davison, A.; Jones, A. G.; Davis, M. A.; Szalda, D. J.; Lippard, S. J. *Inorg. Chem.* **1980**, *19*, 1105-1110.
(8) Davison, A.; Orvig, C.; Trop, H. S.; Sohn, M.; DePamphilis, B. V.; Jones, A. G. *Inorg. Chem.* **1980**, *19*, 1988-1992.
(9) Cotton, F. A.; Davison, A.; Day, V. W.; Gage, L. D.; Trop, H. S. *Inorg. Chem.* **1979**, *18*, 3024-3029.
(10) Hayes, R. L. "The Chemistry of Radiopharmaceuticals"; N. D. Heindel, H. D. Burns, T. Honda, L. W. Brady, Eds.; Masson et Cie: New York, 1978; pp 155-168.
(11) Colton, R. "The Chemistry of Rhenium and Technetium"; Interscience: New York, 1975.
(12) Anders, E. *Annu. Rev. Nucl. Sci.* **1959**, *9*, 203-220.
(13) Magee, R. J.; Cardwell, R. J. "Encyclopedia of Electrochemistry of the Elements"; A. J. Bard, Ed.; Marcel Dekker: New York, 1974; Vol. II, Chapter 4, pp 156-184.

0020-1669/81/1320-3298$01.25/0